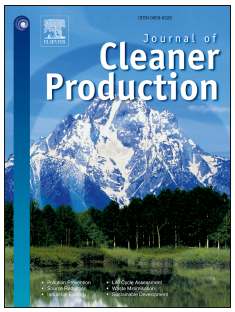

Journal Pre-proof

The role of hydrogen bonding on tuning hard-soft segments in bio-based thermoplastic poly(ether-urethane)s

Paulina Kasprzyk, Hynek Benes, Ricardo Keitel Donato, Janusz Datta

PII: S0959-6526(20)32725-6

DOI: https://doi.org/10.1016/j.jclepro.2020.122678

Reference: JCLP 122678

To appear in: *Journal of Cleaner Production*

Received Date: 8 November 2019

Revised Date: 3 June 2020

Accepted Date: 7 June 2020

Please cite this article as: Kasprzyk P, Benes H, Donato RK, Datta J, The role of hydrogen bonding on tuning hard-soft segments in bio-based thermoplastic poly(ether-urethane)s, *Journal of Cleaner Production*, https://doi.org/10.1016/j.jclepro.2020.122678.

Article title: The role of hydrogen bonding on tuning hard-soft segments in bio-based thermoplastic poly(ether-urethane)s

Authors: Paulina Kasprzyk[1], Hynek Benes[2], Ricardo Keitel Donato[2], Janusz Datta[1*]

Affiliation: [1]Gdansk University of Technology, Faculty of Chemistry, Department of Polymers Technology, 11/12 Gabriela Narutowicza Street, 80-233 Gdansk, Poland

[2]Department of Polymer Processing, Institute of Macromolecular Chemistry, CAS, Heyrovského nám. 2, Prague 162 06, Czech Republic

Corresponding author: Professor Janusz Datta, e-mail address: janusz.datta@pg.edu.pl

The role of hydrogen bonding on tuning hard-soft segments in bio-based thermoplastic poly(ether-urethane)s

Paulina Kasprzyk[1], Hynek Benes[2], Ricardo Keitel Donato[2], Janusz Datta[1*]

[1]Gdansk University of Technology, Faculty of Chemistry, Department of Polymers Technology, 11/12 Gabriela Narutowicza Street, 80-233 Gdansk, Poland

[2]Department of Polymer Processing, Institute of Macromolecular Chemistry, CAS, Heyrovského nám. 2, Prague 162 06, Czech Republic

*Corresponding author. E-mail address: janusz.datta@pg.edu.pl

Abstract

This work describes the preparation of bio-based thermoplastic poly(ether-urethane)s (TPU) via a prepolymer method and investigates the effect of varying the interphase hydrogen-bonding (H-bonding) on physicochemical, thermal and mechanical properties. This was achieved by varying the glycol type and molar ratio of [NCO]/[OH] groups used during the prepolymer chain extending step. The TPUs' chemical structure was analyzed by Fourier Transform Infrared Spectroscopy (FTIR-ATR) spectroscopy, the H-bonding fraction and crystallinity were examined by FTIR, Different Scanning Calorimetry (DSC), X-ray diffraction (XRD) and Polarized light optical microscopy (POM), and their processability was surveyed using the melt-flow index and Matrix-Assisted Laser Desorption/Ionization-Time of Flight Mass Spectrometry (MALDI-TOF-MS). Moreover, a coupled-Thermogravimetric analysis (TGA)-FTIR method provided useful information about thermal degradation and low molecular mass volatile products formed during the TPUs' thermal decomposition. Altogether, this study intends to provide engineers with new insights to obtain environmentally friendly TPU-based polymeric components (from prime materials to process methods), by associating the application of bio-based reactants to the TPU synthesis and understanding the conditions for these bio-TPUs been applied in low-waste processes such as additive manufacturing.

Keywords: phase separation, thermoplastic polyurethanes, bio-based monomers, thermal properties, crystalline structure

1. Introduction

The increase in public environmental awareness, and consequent increase in regulation restrictions, has led to replacement of petrochemical monomers used in polyurethane industry by alternative monomers obtained from renewable sources, e.g., biomass, sugars or vegetable oils (Landim et al., 2019; Parcheta and Datta, 2017). There is plenty of motivation for that since the fossil-based thermoplastic polymers alone are responsible for about 13 million metric tons/year of direct contamination by polymeric solid residues. Moreover, besides been hard to degrade they also undergo incomplete degradation caused by ultraviolet (UV) radiation, mechanical abrasion, and biological processes, producing microplastic polymer particles (Donato and Mija, 2019). Additionally, the substitution of the petrochemical components allows for economic volatility reduction by the decrease in fossil fuel stock utilization. As a result, there is an improvement in economic stability in the countries without access to fossil fuels (Parcheta and Datta, 2017), since bio-based monomers production provides a decrease in the synthesis cost with an increasing amount of production. Moreover, they allow the reduction of energy consumption during production, the reduction of greenhouse gases' emissions (including decreased CO_2 emissions), and the biodegradability improvement (Muellhaupt, 2013). This caused a search for renewable monomers that can replace the usual synthetic monomers, for materials synthesis, without worsening the properties of the final products (de Oliveira et al., 2019; Lligadas et al., 2013).

Thermoplastic polyurethanes (TPUs) are important groups of polyurethanes, obtained by the reaction of polyols, diisocyanates, and chain extenders - usually glycols (Król, 2007). The petrochemical chain extenders and polyols can be replaced by bio-derived compounds such as 1,3-propanediol (PDO), 1,4-butanediol (BDO), and bio-based poly(trimethylene glycol), which are produced by environmentally friendly biotechnological syntheses. PDO is obtained from glucose conversion using a patented microorganism under specific conditions (Adkesson et al., 2003; Emptage et al., 1999), and bio-based polyols, such as poly(trimethylene glycol) (PO3G), for TPU synthesis can be produced by the polycondensation of PDO. BDO is also obtained via a microbiological process by

the direct fermentation of sugars using the metabolic engineering of Escherichia coli, which is a patented fermentation technology from Genomatica (Burk et al., 2008).

TPUs display excellent properties; such as high abrasion resistance, good thermal stability, high tensile strength, and flexibility (Kasprzyk and Datta, 2019). They have increased attention both in basic and applied research because these materials can be easily processed by various methods such as injection molding, extrusion, and blow molding (Lee et al., 2009; Verstraete et al., 2016). The melt flow index is an essential parameter influencing the melt processability, which depends on the number and weight average molecular weight, and polymer structure (Ferg and Bolo, 2013; Guerreiro et al., 2012). Moreover, TPU processability is also facilitated by their good thermal stability and phase transition temperatures (Xie et al., 2019).

TPUs contain repeating units of hard (HS) and soft segments (SS), where HS are derived from diisocyanate and short organic diols, and SS are built by polyols. As a result of thermodynamic incompatibility between the two types of segments, phase separation occurs (Yilgor et al., 2006). Materials with a high degree of microphase separation are characterized by the presence of two glass transition temperatures related to SS (T_{gSS}) and HS (T_{gHS}) (Kasprzyk and Datta, 2018). However, it is worth noting that TPUs never display a complete phase separation, and HS are always partially mixed with SS (Kasprzyk et al., 2019). As a result, the properties of TPUs are sensitive to many factors, such as synthetic (polymerization) procedure, processing method, thermal history, chemical structure, characteristics of the precursors used (e.g. polyols, diisocyanates, chain extenders), solubility parameters, volume fractions of HS and SS, intermolecular interaction between HS and SS, and T_{gSS} (Buckley et al., 2010). This vast property tunability turns TPUs into promising materials for additive manufacturing (AM), which can produce end-use solid objects via layered stacking (Xu et al., 2020). The AM is known as the “third industrial revolution”, since it presents considerable production benefits, including the dramatic reduction of production waste by optimally utilizing materials and energy to produce final components (Ma et al., 2018).

This work explores the use of bio-polyols and bio-glycols to synthesize bio-based thermoplastic poly(ether-urethane)s (TPUs) with controlled ratios of HS and SS, via a two-step solvent-free method. The influence of different [NCO]/[OH] molar ratio and the type of bio-glycols on the TPUs’ properties and processability were studied. Variable TPU compositions significantly affected hydrogen bonding interaction between HS and SS, which allowed us to obtain materials with a wide

range of thermo-mechanical properties and melt flow indexes. The influence promoted by the [NCO]/[OH] molar ratio and the type of bio-glycols on the TPUs' morphology and interphase bonding was also studied, to tune these characteristics by varying simple synthetic parameters and obtaining bio-TPUs with a good balance between processability and final properties.

2. Materials and methods

2.1. Materials

The bio-based poly(trimethylene glycol) (PO3G) (M_n = 2000 g/mol, hydroxyl number 59.1 – 53.4 mgKOH/g) was provided by Allesa (Germany). 4,4'-diphenylmethane diisocyanate (MDI) (NCO content: 33.5%, purity 99.5%) was purchased from Borsed Chem (Hungary). The bio-based glycols: 1,4-butanediol (bio-BDO) (purity 99.8%) and 1,3-propanediol (bio-PDO) (purity 99.7%),were supplied by BASF (Germany) and DuPont Tate&Lyle, respectively. The catalyst 1,4-diacabicyclo[2.2.2]octane (DABCO) was purchased from Sigma-Aldrich (Poland).

2.2. Thermoplastic poly(ether-urethane)s (TPUs) synthesis

TPUs were prepared using a two-step prepolymer method. Initially, a prepolymer was synthesized by reacting to the PO3G polyol with an excess amount of diisocyanate at 85^{o}C for 3 h under vacuum. The percentage of the unreacted NCO groups in prepolymer was equaled 7%, which was determined according to the ISO 14896:2010 standard. Secondly, a chain extender and a catalyst (0.3% DABCO) were added to the prepolymer, and the mixture was stirred for 30 s. For TPU syntheses, molar ratios of [NCO]/[OH] groups of 0.9, 0.95 and 1.0, and two bio-glycols (BDO and PDO) were used. Finally, the materials were post-cured in a laboratory oven at 100^{o}C for 24h. A summary of the synthetic procedures is presented in Figure 1.

The materials were encoded as follows; the first part of the symbol corresponds to the bio-glycol used (B for bio-BDO glycol and P for bio-PDO glycol), while the second part refers to the [NCO]/[OH] molar ratio during the prepolymer chain extending step, e.g., the sample coded as P_0.9 was obtained using bio-PDO and presents a [NCO]/[OH] molar ratio of 0.9.

Figure 1. The synthesis of bio-based thermoplastic TPUs.

2.3 Methods

Size exclusion chromatography (SEC) was performed to determine the number (M_n) and weight average (M_w) molecular weights, as well as the dispersity. A chromatographic system equipped with a refractive index detector (Shodex, Japan), UV-Vis detector (λ = 254 nm, LCD 2084, Ecom, Czech Republic) and a set of three columns (PLgel with a particle size of 10 μm, pore size: 50/10E3/10E4 Å, 300x7.5 mm, Polymer laboratories, UK) was used. Tetrahydrofuran was applied as the eluent at a 1 ml/min flow rate, and the calibration was done on polystyrene standards.

Fourier transform infrared spectroscopy (FTIR) was carried out using a Nicolet 8700 FTIR spectrophotometer (Thermo Electron Co., USA) on attenuated total reflection (ATR) mode. The spectra were recorded at the room temperature for wavenumbers ranging from 500 to 4000 cm^{-1} at 4 cm^{-1} nominal resolution with 64 scans, using the normalized spectra for analysis. To calculate the degree of phase separation, spectra were analyzed in the 1760 – 1680 cm^{-1} region by deconvolution of the carbonyl peaks using Origin software. The degree of phase separation (DPS) and the degree of phase mixing (DPM) were calculated according to the equations (1-3):

$$DPS = \frac{R}{R+1} \quad (1)$$

$$R = \frac{A_b}{A_f} \quad (2)$$

$$DPM = 1 - DPS \quad (3)$$

Where: R is the carbonyl hydrogen bonding index; A_b is the absorption intensity of hydrogen-bonded carbonyl; A_f is the absorption intensity of free carbonyl.

Thermogravimetric analysis (TGA) coupled with Fourier transform infrared spectroscopy (FTIR) of released gases was performed using a Pyris 1 TGA (PerkinElmer) coupled with an IR spectrometer Spectrum 100T FT-IR (PerkinElmer) through a transfer line TL 8000 (PerkinElmer). The analyses were

performed under a 25 mL min^{-1}nitrogenflowwithin the temperature range of 35 – 700 °C and at a heating rate of 10 °C min^{-1}. The infrared spectroscopic cell and the coupling system to TGA were kept at 270 and 260 °C, respectively, to prevent the condensation of evolved gases or vapors. FTIR spectra were continuously collected during the whole analysis, and they were recorded within the range of 650 - 4000 cm^{-1}, at 2 scans per spectrum at 4 cm^{-1} resolution.

Dynamic mechanical and thermal analysis (DMTA) was carried out, under the flexural mode, following ASTM D4065:2012 using the DMA Q800 analyzer (TA Instruments) within the temperature range of-100 and 150^{o}C, at a heating rate of 4^{o}C/min and the frequency of 10 Hz. The measurements provided information about the systems' storage (E') and loss (E'') moduli, and the glass transition temperatures of the SS based on the maximum tan delta peak (T_{α}).

Differential scanning calorimetry (DSC) was performed using a Q 2000 calorimeter (TA Instruments). The measurements were carried out in the heating-cooling-heating cycle from -90 to 250^{o}C, and the heating rate was 10^{o}C/min and under a nitrogen purge of 50 ml/min. The sample weight was approximately 6 mg, and the data was collected from the first cooling ramp and the second heating ramp to exclude the samples' thermal history. Analyses were performed twice to ensure the data consistency within the thermal range performed.

X-ray diffraction (XRD) was performed with a high-resolution diffractometer Explorer (GNR Analytical Instruments, Italy) equipped with a one-dimensional silicon strip detector Mythen 1K (Dectris, Switzerland). The CuKα radiation (wavelength λ= 1.54 Å) was produced by a sealed X-ray tube operated at 40 kV and 30 mA and monochromatized with Ni foil (β filter). The measurements were performed in Bragg-Brentano geometry in the range of 2θ = 5 – 70° with a step 0.1°. The exposure time at each step was 15 s.

The mechanical properties in static conditions were investigated on Zwick Z020 tensile testing machine, according to ISO 37:2007 standard. The dumbbell specimens were stretched at a cross-head speed of 100 mm/min, at room temperature. The hardness measurements were carried out using an electronic Shore type A Durometer, following ISO 868:2005 standard. The results were determined as the average of ten measurements.

Melt flow index (MFI) of bio-based thermoplastic polyurethanes were measured using Zwick/Roell plastometer, under ISO 1133. The evaluations were conducted with a 5.0 kg load at three different temperatures, i.e. 170, 175, and 180 °C.

Polarized light optical microscopy (POM) images were obtained, to differentiate the soft and hard segments present before and after a thermal treatment up to 250 °C (under vacuum) followed by a controlled cooling at 2 °C/min down to the room temperature. The images were obtained with a Canon EOS 650D camera coupled with a Zeiss Opton Photomicroscope III, using Planapo 63 objective lenses. The POM imageswereanalyzedusingImageJsoftwareforquantitativeevaluationofthe HS domain sizes and area contribution. Image areas of 150 x 150 μm areas were analyzed, where the measurements were repeated five times and averaged for ensuring the reliability of the results.

MALDI-TOF mass spectra were acquired with Ultraflex (Bruker Daltonics, Bremen, Germany) in the positive ion reflection mode, using delayed extraction. The spectra were the result of 30 000 shots with a DPSS, Nd: YAG laser (355 nm, 1000 Hz). External calibration was used. The samples were prepared by the dried droplet method. Chloroform solutions of the samples (10 mg/mL), the matrix: DHB (2,5-dihydroxybenzoic acid; 20 mg/mL), and the cationization agent: sodium trifluoroacetate ($NaCF_3COO$; 10 mg/mL) were mixed in the respective volume ratio 4:20:1.1 μL. The mixture was deposited on a ground-steel target plate, and the analyzed drop was dried at an ambient atmosphere.

3. Results and discussion

The weight (M_w) and number (M_n) average molecular weights and the dispersity (*Đ*) indexes, as obtained by SEC, together with the chemical compositions and the hard segment (HS) contents of all TPU samples were displayed in Table 1. The formation of TPUs with high M_w and M_n was observed, with broad molecular weight distribution, where both the molecular weight and the dispersity proportionally increasing with [NCO]/[OH]. Consequently, samples B_1.0 and P_1.0 presented both the highest molecular weights and dispersities, however, the samples with the lowest [NCO]/[OH] during the prepolymer chains extending step displayed the highest contents of HS.

Table 1. Molar ratio, HS content, molecular weights, and dispersity of synthesized bio-based TPUs.

Label	[NCO]/[OH]	HS [%]*	M_n	M_w	Đ	M_n theoretical
B_0.9	0.9	34.6	20	44 300	2.21	10365
B_0.95	0.95	34.3	24	59 900	2.45	19374
B_1.0	1.0	34.1	31	84 500	2.66	86648
P_0.9	0.9	34.1	18	38 300	2.06	10182
P_0.95	0.95	33.8	23	50 500	2.14	18928
P_1.0	1.0	33.5	30	71 800	2.35	85470

***[NCO]/[OH]**–the molar ratio of NCO and OH groups during the prepolymer chains extending step; **HS** – the content of hard segments defined as the ratio of the mass of non-polyol components to the total mass of the polymer; **M_n** – number average molecular weight; **M_w** – weight average molecular weight, **Đ**–dispersity, **M_n theoretical** – calculated using Carothers equations (Yilgor et al., 2003).

The influence of the bio-glycol type and [NCO]/[OH] on the chemical structure, and the DPS of the TPUs obtained were examined by FTIR and the spectra were presented in **Figure 2a**. Without spectra normalization, all synthesized materials showed the characteristic groups for polyurethanes, suggesting a quite similar chemical structure. The absorption bands related to NCO (2270 cm^{-1}) and OH groups (3300 – 3500 cm^{-1}) were not observed, thus suggesting the complete monomer consumption. The –NH stretching vibrations of the urethane groups were shifted to a characteristic area representative to H-bond formation at the wavenumbers between 3411 and 3210 cm^{-1}, with the maxima at 3320 cm^{-1} (Prisacariu et al., 2013). This band's intensity increased with decreasing the [NCO]/[OH] molar ratio (Figure 2a), which would represent an increase of H-bonded groups. Additionally, the maximum at 3320 cm^{-1} was generally more intense for the materials based on bio-BDO. The bimodal band with the maxima at 2857 cm^{-1} and 2960 cm^{-1} was assigned to the CH asymmetric and symmetric stretching in the CH_2 groups, respectively, while the deformation vibrations of the C-H groups were observed at 1410 cm^{-1}. The carbonyl groups (C=O) stretching vibrations were observed in the range between 1660 and 1740 cm^{-1} (Kopczyńska and Datta, 2016; Mizera and Ryszkowska, 2016). In this region, three bands were usually observed, which were associated with: I) H-bonded carbonyl groups in ordered HS(1685 – 1706 cm^{-1}); II) H-bonded carbonyl groups in a disordered region (1714-1719 cm^{-1}); III) free carbonyl groups (1730 cm^{-1}) of SS (Niemczyk et al., 2017). Moreover, bands associated with the urethane groups' N-H out-of-plane bending (1599 cm^{-1}) and C–N stretching vibration (1520 cm^{-1}), and with the polyether polyol's free ether bond (strong, 1100 cm^{-1}) were also observed. In the latter, two characteristic bands were visible and were associated with:

I) antisymmetric stretching vibration of non-associated ether groups (1100 cm^{-1}); II) H-bonding between N-H and C-O-C groups (1062 cm^{-1}). The multiple bands in the range 1180 - 1280 cm^{-1} was connected with C-O stretching vibrations of the urethane groups in the amide III region (Saralegi et al., 2013). Generally, with the increasing [NCO]/[OH] the band maximum was shifted towards higher values. Once again, a correlation between band intensity and [NCO]/[OH] was observed, where the carbonyl band increases with increasing [NCO]/[OH] during the prepolymer chains extending step (see **Figure 2** and Supplementary Information **Figure S1**), and yet again the TPUs based on bio-BDO displayed higher intensity than the ones based on bio-PDO.

Figure 2. a) FTIR-ATR spectra of bio-based TPU systems, b) Gauss model fitting of sample B_0.95. The solid line represents the sum of the overlapped peak-components (I – III), and the dashed lines represent the deconvoluted distributions.

The band intensities and wavenumber shifts in the C=O region provided useful information about the microphase separation within the bio-TPUs. **Figure 2b** shows the deconvoluted carbonyl peak areas with band positions at 1731, 1717 and 1700 cm^{-1}(marked as Peak I, II, and III) related to free and H-bonded C=O within SS and HS, respectively. The calculated area fractions of the deconvoluted bands were given in **Table 2**. The exact band positions indicated only small differences among the materials containing different glycols and [NCO]/[OH]values. It could be concluded that more than 70% of the HS was microphase separated, while only 30% of the HS seemed to be mixed within the polyether polyol matrix. The bio-TPUs prepared by using bio-BDO presented a higher fraction of H-bonded carbonyl groups than ones with bio-PDO, as a probable consequence of the symmetric structure of bio-BDO. Additionally, materials prepared with lower [NCO]/[OH] had a higher fraction of H-bonded C=O groups. However, the amount of H-bonded carbonyl groups was affected not only by the content of HS but also by the symmetry of the chain extender used.

Table 2. Deconvolution of the FTIR absorbance bands in the range between 1750 and 1660 cm^{-1}, occurring in the prepared TPUs.

Symbol	**-C=O band**			**DPS**	**DPM**
	Peak I: free C=O	**Peak II: H-bonded amorphous region**	**Peak III: H-bonded in ordered HS**		

	υ [cm^{-1}]	f [%]	υ [cm^{-1}]	f [%]	υ [cm^{-1}]	f [%]		
B_0.9	1730.51	23.93	1716.85	4.85	1699.81	71.23	0.715	0.285
B_0.95	1730.62	25.83	1717.19	4.42	1699.98	69.75	0.690	0.310
B_1.0	1730.68	27.14	1717.25	4.21	1700.11	68.65	0.675	0.325
P_0.9	1730.10	23.94	1716.23	9.72	1702.38	66.35	0.776	0.224
P_0.95	1730.15	28.05	1716.28	9.13	1702.10	62.83	0.736	0.264
P_1.0	1730.68	30.29	1717.65	8.50	1702.02	61.22	0.718	0.282

***υ** - location of maximum absorbance; **f** – fraction; **DPS** – degree of phase separation; **DPM** – degree of phase mixing.

Regarding the TPUs' thermal properties, five thermal events (one glass transition temperature, two exotherms, and two endotherms) could be distinguished from the DSC runs (Figure 3), and the results are summarized in **Table 3**.

The T_{gSS} were detected around -61^{o}C and were slightly increased for TPUs with higher M_w. Moreover, since T_{gSS} is strongly dependent on the degree of miscibility between HS and SS (Eceiza et al., 2008; Niemczyk et al., 2017), TPUs with higher [NCO]/[OH] values displayed higher T_{gSS}. Consequently, the TPUs encoded B_1.0 and P_1.0 presented the highest T_{gSS} values, as higher contents of HS are embedded in the SS, thus decreasing the DPS as confirmed by FTIR-ATR.

The DSC cooling curves gave information about the TPUs' crystallization behavior. The decrease in [NCO]/[OH] promoted considerably the crystallization kinetics of the bio-based TPUs, while higher [NCO]/[OH] displayed broader peaks (higher DPM), as evidenced by the DSC's exothermic crystallization peaks. Sample B_0.9 displayed a 20 $^{\circ}$C higher crystallization temperature (T_c) and a higher crystallization enthalpy change (ΔH_c), in comparison to samples B_0.95 and B_1.0. Additionally, TPUs prepared using bio-PDO as chain extenders generally showed higher ΔH_c than the bio-BDO-based ones.

The second heating curves of DSC exhibited a relatively sharp exothermic peak at about -20^{o}C resulting from the cold-crystallization of the SS (Righetti, 2017), followed by the endotherm at 10^{o}C associated with their melting temperature (T_m). This phenomenon was exclusive to TPUs with [NCO]/[OH] = 0.9 and 0.95, suggesting the ability of these TPU formulations to form molar ratio-dependent ordered structures. The T_m (displayed upon heating) of SS was slightly increased as [NCO]/[OH] was also increased (within the temperature range between 0 to 12^{o}C). The T_m at higher

temperatures (170 - 240°C) were connected with the dissociation of a long-range ordering, which was related to the mixing between HS and SS. These multiple endotherms at higher temperatures were also associated with the melting of HS crystallites, phase-separated into different domain sizes, and microcrystalline structures upon cooling (Hossieny et al., 2017; Niemczyk et al., 2017). A similar phenomenon was also observed by Eceiza *et.al.*, which prepared model rigid segments based on MDI and BDO and observed three endotherms at high temperatures (200 - 240°C) related to the melting of HS (Eceiza et al., 2008). The registered melt-endotherms confirmed the formation of the broad size distribution of HS crystallites, as also observed in the T_c profiles at the cooling curves (Figure 4). Especially samples B_0.9, B_0.95 and P_0.9 displayed increased high-temperature endothermic peaks, and their shift to higher temperatures, as a result of better HS ordering and formation of stronger and more stable HS domains. Moreover, the samples B_0.9 and B_0.95 also presented defined bimodal T_c behaviors, indicating the formation of more than one crystallite type.

For this reason, these two systems were analyzed using polarized light optical microscopy (POM) for observing the HS size and distribution, before and after being thermally treated above the T_m followed by controlled slow cooling (2°C/min). This procedure was applied to induce different crystallization behavior. This thermal treatment considerably increased the number of HS within the TPU network, however, no considerable change in HS size was observed (Figure 3c and d). Similar results have been previously described by other authors, where the HS aggregate diameters were between 0.4 and 1.5μm (areas ~ 0.502 - 7.080 μm^2) and HS aggregates volume fraction between 8 and 21% (Lvii et al., 2012). Altogether, the bio-based TPUs that presented higher microphase separation showed higher total ΔH_c and ΔH_m, also showing a greater tunability during the crystallization processes.

Table 3. Summary of DSC results of the bio-based TPUs.

Sample	**T_{gss} (°C)**	**T_c (°C)**	**ΔH_c (J/g)**	**Total ΔH_c (J/g)**	**T_m (°C)**	**ΔH_m(J/g)**	**Total ΔH_m (J/g)**
B_0.9	-62.1	-12.1 122.4	3.3 6.1	9.3	8.6 178.5 193.0 212.5	3.5 4.9 0.6 0.6	9.7

B_0.95	-61.4	118.5	8.7	8.7	9.7 181.4 203.8 221.0	0.5 6.2 0.5 0.1	7.3
B_1.0	-59.6	104.6	7.0	7.0	2.0 173.2 204.8	0.03 5.4 0.1	5.5
P_0.9	-63.3	-10.2 162.4	7.1 8.8	15.9	9.8 176.7 227.0	9.2 2.1 2.2	13.7
P_0.95	-61.6	-5.4 128.2	0.8 8.5	8.5	11.5 193.4	1.0 7.6	8.6
P_1.0	-60.1	129.1	6.5	6.5	1.0 195.4	0.1 6.0	6.1

***ΔH_m** – melting enthalpy; **ΔH_c** – crystallization enthalpy; **T_c** – crystallization temperature; **T_m** – melting temperature; **T_{gSS}** – glass transition temperature of the soft segments.

Figure 3. DSC thermal transition curves of the second heating (a) and first cooling (b) ramps of the bio-based TPUs. POM microphotographs of samples B_0.9 (c), and B_0.95 (d), before (left) and after (right) a thermal treatment at 250 °C (under vacuum) followed by a controlled cooling at 2 °C/min. A_{HS} is the area and $A_{\%HS}$ is the area fraction (and an estimation of the volume fraction) of HS aggregates.

The TGA results were displayed in **Figure 4** and **Table 4,** where$T_{5\%}$ was assessed as the initial degradation temperature. As a general trend, bio-BDO-based systems presented $T_{5\%}$ 10 °C higher than bio-PDO ones. TPUs often present two decomposition stages (Lei et al., 2017): a first degradation step with a maximum at 330-350°C, referring to the HS decomposition; and a second degradation step around 425 °C, connected to the SS decomposition. All TPUs prepared in this work followed this characteristic, and the rate of weight loss was dependent on [NCO]/[OH]. With the increase of [NCO]/[OH] the maximum weight loss rate for the first decomposition step decreases, while the one for the second decomposition step increases. This could be correlated with the HS content in both bio-BDO- and bio-PDO-based systems since all TPUs with a higher HS content also

307 presented a higher weight loss rate for the first decomposition step and a lower weight loss rate for the
308 second decomposition step (Table 4).

309 Thermal stability depended on [NCO]/[OH] and the type of bio-glycols during the chain
310 extender step. With the increase of [NCO]/[OH] the thermal stability slightly increased. TPUs based on
311 bio-BDO displayed higher thermal stability than the ones based on bio-PDO, which could be related to
312 a more symmetric structure of bio-BDO in comparison to bio-PDO. All the prepared systems were
313 thermally degraded and carbonized above 500^{o}C leaving only char residue, which varied negligibly for
314 bio-BDO and only slightly more for bio-PDO.

315

316 **Table 4.** Thermal degradation profiles of the bio-based TPUs obtained by TGA.

Sample	**$T_{5\%}$ [^{o}C]**	**$T_{10\%}$ [^{o}C]**	**$T_{50\%}$ [^{o}C]**	**$T_{90\%}$ [^{o}C]**	**Char (wt.% at 650^{o}C)**	**I step degradation**		**II step degradation**	
						T_{max}[^{o}C]	**DTG_{max} [%/min]**	**T_{max} [^{o}C]**	**DTG_{max} [%/min]**
B_0.9	325.8	338.1	403.0	437.4	3.13	349.5	-6.72	422.2	-15.07
B_0.95	326.1	339.0	403.9	437.6	2.77	348.4	-6.70	423.4	-15.13
B_1.0	327.3	339.5	407.5	441.9	3.21	348.1	-6.39	423.2	-15.29
P_0.9	315.9	327.6	413.8	444.1	3.29	332.4	-4.95	427.2	-16.24
P_0.95	316.5	328.7	415.8	458.1	4.97	333.3	-4.82	427.4	-16.61
P_1.0	317.4	331.0	416.0	457.2	4.89	332.2	-4.71	427.6	-17.00

317

318 **Figure 4.** TGA and DTG curves of the bio-based TPUs.

319

320 Coupled TGA-FTIR analysis provided a more detailed description of the degradation
321 processes, by the continuous monitoring of the thermal degradation products by FTIR. The spectra
322 were recorded at the maximum evolution rate for each decomposition step of systems composed of
323 different bio-polyols (B_0.95 and P_0.95) (Figure 5). There are three main thermal decomposition
324 pathways for the urethane linkages: I) the dissociation to isocyanates and alcohols; I) the dissociation
325 to primary amines, olefins and carbon dioxide, and; III) the formation of secondary amines with the
326 elimination of carbon dioxide (Pielichowski and Leszczy, 2004).

Taking that into account, the spectra corresponding to the volatile products recorded during the first and second mass loss steps of systems B_0.95 and P_0.95 were very similar. The spectra collected at 348 and 333^{o}C (first degradation step) showed multiple bands associated with the symmetric and asymmetric C-H stretching vibration from isocyanate and hydrocarbons (2860 – 2970 cm^{-1}), with carbonyl groups (1720 cm^{-1}), and with C-O-C vibrations (1070 cm^{-1}). The bands within the range 4000 – 3500 cm^{-1} are be related to the N-H and O-H stretching vibrations (Cervantes-Uc et al., 2009), while the bands at 918 and 647 cm^{-1}are associated with the C-H bending vibrations of aromatic rings (Yang et al., 2012). At the second degradation step (423 and 427^{o}C), more intense bands at 3641-3786 cm^{-1}, 2670 – 2960 cm^{-1}, 1730 cm^{-1}, 1510 – 1340 cm^{-1}, 1100 cm^{-1} and 911 – 995 cm^{-1} were observed. They were mainly connected to the SS thermal decomposition, indicating that their volatile decomposition products were aliphatic ethers, aldehydes, and carbon monoxide. The bands at 2780, 2745, and 2810 cm^{-1} were connected with C-H stretching vibrations, the multiple peaks in the range 1660 – 1760 cm^{-1}with C=O stretching vibrations, and the band at 954 cm^{-1} with C-H bending vibrations of aldehyde groups. The band at 1100 cm^{-1}was attributed to C-O stretching vibrations, and the bands at 2960 – 2860 cm^{-1} to C-H stretching vibrations of the ether groups. The multiple peaks with several maxima at 1479, 1429, 1335 cm^{-1} originated from the CH_2 and CH_3groups from polyols. Finally, the band in the range 3573 – 3768 cm^{-1} was attributed to O-H stretching vibrations from alcohol (Cervantes-Uc et al., 2009; Herrera et al., 2002).

Figure 5. FTIR spectra recorded during the 1st and 2nd mass loss step for the bio-TPU systems B_0.95 and P_0.95.

Since the DSC analyses of the TPU systems indicated some degree of ordering, XRD characterizations were also performed. Considering that broad Gaussian peaks correspond to less ordered arrangements and defined sharp peaks correspond to crystalline domains (Lei et al., 2017), all bio-TPUs displayed an overall amorphous profile with the presence of some ordered/crystalline structures **(see SI, Fig. S2)**. The crystallinity seems to be originated from the bio-polyols used since the neat polyol precursors presented crystalline peaks at 2θ ~14.4, 19.4, 20.6, 22.6, 23.7, 24.5^{o}. The TPUs exhibited three weak diffraction patterns at about 11.5, 20.2 42.4^{o}, among which could be

observed a series of small peaks at 2θ ~11.0, 19.2, 20.6, and 24.3°. It worth noting that the crystalline structures observed herein are provided only by the SS since it is necessary to anneal the TPUs for observing also the HS (Fang et al., 2014; Lei et al., 2017), which was not the case in this study.

Regarding the TPUs' mechanical properties, the DMTA results were presented in **Table 5** and the shifts in storage modulus (E'), loss modulus (E'') and the E"/E' ratio (tan δ) (as a function of the temperature) were displayed in **Fig. 6**. The transition temperatures detected by DMTA presented a good correlation with the DSC data. Initially, the E' decreased significantly at temperatures higher than -30°C, matching with the T_{gSS} observed by DSC. Subsequently, it could be observed the maximum peak in the tan δ, referring to the $T_{\alpha}$of the SS, herein also denoted as T_{gSS} (Table 5). Additionally, above the T_{gSS} the E' decreased steadily up to -20°C, followed by a sudden E' increase coinciding with the cold crystallization of the SS observed for the same systems. Moreover, DMTA detected a weak secondary thermal transition in the temperature range from 75 to 100°C, which was connected with the glass transition of hard segments (T_{gHS}).

The value and shape of the tan δ curve (vs. temperature) provided information about the damping capacity (Beniah et al., 2016; Prisacariu, 2011). The TPUs prepared using bio-PDO as chain extenders displayed the highest tan δ values. Moreover, tanδ also depended on [NCO]/[OH] and decreased with increasing [NCO]/[OH]. Therefore, TPUs with lower H-bond content and higher M_w were less effective for damping vibrations. Although all TPUs had similar tan δ peak widths, the ones with [NCO]/[OH] = 0.9 and 0.95 presented an additional peak above 75°C, which was connected to the T_{gHS}.

Table 5. DMTA results of prepared TPUs.

Sample	**T_{gSS} [°C] (DMTA)**	**tan δ**	**E' $_{max}$ [MPa]**	**E' [MPa] at temp.**			**T_{max} of E''**	**E'' $_{max}$ [MPa]**
				T_{gSS}	**25°C**	**100°C**		
B_0.9	-37.8	0.42	3020	420	42	14	-46.2	458
B_0.95	-36.4	0.47	2989	389	41	18	-46.1	449
B_1.0	-35.7	0.50	3010	370	40	20	-45.4	418
P_0.9	-38.2	0.49	3214	405	40	13	-46.6	434
P_0.95	-36.7	0.52	3198	381	39	12	-46.2	430

P_1.0	-35.9	0.54	3276	372	38	16	-45.7	411

378 ***T_{gss}** – glass transition temperature of the soft segment; **E' $_{max}$** – maximum value of storage modulus; **E'** –
379 storage modulus; **E''** – loss modulus.

380

381 **Figure 6.** DMTA curves of the TPUs based on (a) bio-BDO and (b) bio-PDO as a function of the
382 temperature.

383 Regarding the general mechanical properties, the young's modulus (*E*) of the TPUs increased
384 with decreasing [NCO]/[OH]. TPUs based on bio-BDO presented the best mechanical performances
385 with *E* ranging between 33.4 and 38.5 MPa, while for bio-PDO-based ones it ranged from 29.9 to 33.2
386 MPa (**Table 6)**. As shown in Tables 1 and 2, the materials prepared with bio-BDO presented a higher
387 content of H-bonded carbonyl groups and HS. Thus, *E* increased proportionally with increasing the
388 interfacial H-bonding, which also explained the higher stiffness observed by DMTA (Figure 6 and
389 Table 5), caused by the more restricted mobility within the TPU networks (Saralegi et al., 2013).
390 However, although increasing [NCO]/[OH] caused a reduction in *E*, the tensile strength (TS_b) and the
391 elongation at break (***ε***) increased, reaching tensile properties comparable to those of highly stretchable
392 TPU-based composites applied as strain sensors (Duan et al., 2018). The *TS* and ***ε*** of bio-PDO-based
393 TPUs ranged from 7.2 to 24.6 MPa and from 189 to 680%, respectively, while bio-BDO-based ones
394 ranged from 7.7 to 28.2 MPa and from 200 to 768%, respectively. Moreover, system B_0.9 displayed
395 higher hardness than systems B_0.95 and B_1.0, which could be explained by the more abundant H-
396 bonding and HS caused by the lower [NCO]/[OH] during the prepolymer chain extension step. The
397 same relationship was also found concerning the hardness of TPUs prepared with bio-PDO. The
398 TPUs densities were strongly dependent on the monomer densities, where TPUs prepared with bio-
399 PDO had a higher density than the ones with bio-BDO. Moreover, for synthesizing TPUs with
400 [NCO]/[OH] = 0.9 it was necessary the use of larger glycol amounts (chain extenders) associated with
401 the prepolymer, consequently, decreasing the density with increasing [NCO]/[OH].

402

403 **Table 6.** Summary of mechanical properties (***TS_b*** and ***ε***), hardness, and density of the bio-TPUs.

Sample	***TS_b [MPa]***	***ε [%]***	***E [MPa]***	***H [°ShD]***	***d [g/cm^3]***

B_0.9	7.7 ± 0.2	200 ± 21	38.5 ± 0.2	80.1 ± 0.4	1.138 ± 0. 012
B_0.95	20.0 ± 1.5	621 ± 18	37.0 ± 0.9	82.6 ± 0.1	1.135 ± 0 .003
B_1.0	28.2 ± 1.3	768 ± 23	33.4 ± 1.1	83.3 ±0.2	1.131 ± 0. 011
P_0.9	7.2 ± 1.2	189 ± 14	33.2 ± 1.1	80.6 ± 0.3	1.162 ± 0. 010
P_0.95	18.4 ± 1.0	589 ± 31	30.7 ± 0.2	82.0 ± 0.2	1.160 ± 0 .009
P_1.0	24.6 ± 2.1	680 ± 20	29.9 ± 0.8	84.1 ± 0.2	1.157 ± 0 .009

404 ***TS_b**– tensile strength; **ε**- elongation at break; **E** – Young moduli; **H** – hardness; **d** – density.

405

406 To prospect the TPUs applicability in processes demanding specific melt-behavior, such as
407 injection molding or additive manufacturing, the materials' melt flow indexes (MFI) were characterized
408 (**Table 7**). As expected, the MFI values were dependent on the TPUs' molar mass, [NCO]/[OH] and
409 the temperature, decreasing with increasing [NCO]/[OH]. The M_w (Table 1) has probably a major role
410 in this case since it is well-described that materials presenting higher M_w will also be more viscous
411 (Wirpsza, 1993), requiring higher reprocessing temperatures. Bio-PDO-based TPUs presented
412 generally higher MFIs than bio-BDO-based ones, showing also a dependency on the polymer
413 backbone formed by the different polyols. Almost in a complementary fashion, at 170°C both MFI and
414 the melt volume flow rate (MVR) increased in the following order: B_1.0 < B_0.95< B_0.9 < P_1.0 <
415 P_0.95 < P_0.9 (Table 7).

416 Interestingly, many of the TPU systems presented MFI values close to the ideal for fused
417 deposition modeling (FDM) additive manufacturing, which for the most commonly used thermoplastic
418 polymer, poly(lactic acid), is MFI = 10g/10min (Wang et al., 2017). Moreover, a sufficiently high MFI is
419 required for an acceptable FDM printing quality, which can be obtained by altering the melting set
420 point. However, from an industrial point of view, materials within this MFI range are preferred,
421 especially if they allow control over the crystallinity and plasticizer type. Since the sole focus on MFI is
422 insufficient, and the plasticizer type and crystallinity also play a role after the polymer melt deposition,
423 we carefully analyzed the bio-TPUs with the best crystallinity controls (B_0.9 and B_0.95) using SEC
424 and MALDI-TOF mass spectroscopy. These analyses enabled us to detect any monomeric/oligomeric
425 residue that could promote the self-plasticization of the bio-TPUs, also acting as coupling agents
426 between HS and SS (Fig. 7).

427

428 **Table 7.** Temperature-dependent MFI and MVR results of the bio-TPUs.

Sample	170 °C, 5kg		175 °C, 5kg		180 °C, 5kg	
	MFI[g/10min]	MVR [g/10min]	MFI[g/10min]	MVR [g/10min]	MFI[g/10min]	MVR [g/10min]
B_0.9	16.2 ± 0.2	16.4 ± 0.3	38.2± 0.4	38.3± 0.2	62.8 ± 0.2	63.2 ± 0.2
B_0.95	10.2 ± 0.3	10.5 ± 0.2	12.5 ± 0.2	12.8 ± 0.3	26.3 ± 0.1	26.6 ± 0.3
B_1.0	7.2 ± 0.2	7.4 ± 0.5	10.6 ± 0.3	10.9 ± 0.4	21.2 ± 0 .1	21.5 ± 0.1
P_0.9	37.3 ± 0.4	37.5 ± 0.3	56.1 ± 0.1	56.4 ± 0.4	89.1 ± 0.9	90.2 ± 1.0
P_0.95	25.6 ± 0.3	25.4 ± 0.8	32.5 ± 0.5	33.0 ± 0.1	61.3 ± 0.7	61.5 ± 0.6
P_1.0	17.7 ± 0.1	18.2 ± 0.3	28.7 ± 0.2	29.2 ± 0.2	41.2 ± 0.5	41.5 ± 0.7

429 **MFI** - the melt (mass) flow index, **MVR** - melt volume flow rate

430

431 **Figure 7.** MALDI-TOF spectra of systems a) B_0.9 and b) B_0.95 highlighting the repetitive low
432 molecular mass units representing monomeric/oligomeric species in the final TPUs, and c) SEC
433 results of systems B_0.9 and B_0.95, where M_{pn} represents M_n (g/mol) of the nth peak.

434

435 The MALDI-TOF analyses confirmed the presence of several repetitive mass units below m/z
436 = 3000, presenting a bimodal repetition representative of the TPU's SS (m/z ~ 58) and HS (m/z ~
437 340), in both systems B_0.9 (Fig. 7a) and B_0.95 (Fig. 7b). These results suggest that small fractions
438 of these TPUs only reach the oligomeric state or form cyclic structures during the polymerization
439 process. The presence of oligomers or cyclic structures was also detected by SEC (Fig 7c)
440 constituting about 4% of the total mass in B_0.90 and 3% in B_0.95. These are considerable amounts
441 when concerning plasticization and compatibilization, increasing the interphase between the HS and
442 SS within the bio-TPUs. The presence of these oligomers could help to explain both the relatively high
443 MFI values (Table 7) and the thermal dependent variation of phase-separated HS (Fig. 3). However,
444 these oligomeric species seem to be strongly H-bonded within the HS-SS interphase, allowing the
445 sustenance of good mechanical properties even with occurring plasticization. Taking that into account,
446 the system B_0.95 seemed to be a good example of properties balance for the application in FDM 3D

printing, since it presented an ideal MFI value (10.2g/10min) at a moderate printing temperature (170 °C), and would produce a printed TPU part with good E (37 MPa), TS_b (20 MPa) and ε (621%).

4. Conclusion

Bio-based TPUs with [NCO]/[OH] molar ratios ranging from 0.9 to 1.0 were successfully synthesized using a two-step method, where the molecular weight of the TPUs was inversely proportional to [NCO]/[OH]. Also, the type of bio-glycol used (bio-butanediol, BDO or bio-propanediol, PDO) and [NCO]/[OH] affected the degree of phase separation (DPS) and the H-bonding within the TPU matrix. Although all the synthesized TPUs exhibited (micro)phase-separated morphology, the highest DPS was observed for the bio-BDO-based TPUs. Moreover, the Bio-BDO-based TPUs displayed the highest tensile strengths and elongations at break, but at the same time, the lowest melt flow indexes (MFI) due to the presence of oligomers (residual from the synthetic process) acting as plasticizers and hard (HS) / soft (SS) segment coupling agents. Interestingly, this allowed obtaining bio-TPUs with a broad range of MFI values, including within the ideal range for FDM 3D printing. Additionally, all prepared TPUs presented good thermal stability (up to 315^{o}C), with a two-step thermal degradation associated with the decomposition of their HS and SS.

Altogether, the integrated control of the H-bonding, phase-separation, and plasticization/compatibilization via simple synthetic parameters allowed obtaining bio-TPU materials that present good thermomechanical properties in the solid-state while also presenting ideal processability parameters. Consequently, this work not only evaluated the optimum synthesis conditions but also correlated them with the resulting structural effects and the systems' processability, prospecting their applications. Moreover, it was demonstrated that the most application-effective TPU systems are not necessarily the ones with the best bulk thermomechanical properties, hopefully allowing for competitive applications of these bio-based systems into the emerging market of additive manufacturing.

The next challenge to be addressed, associated with these systems, is the formulation of a fully (100%) bio-based TPU that is specifically designed for 3D printing. This would further decrease

the environmental impact of additive manufacturing, while still being competitive with currently commercially available petroleum-based TPUs.

Acknowledgment

The authors wish to thank BASF (Germany) and Allesa (Germany) for kindly providing the bio-based 1,4-butanediol and the bio-based polytrimethylene polyol. The authors are also thankful to Zuzana Walterová for the MALDI-TOF MS measurements and Magdalena Konefal for the XRD measurements.

Conflict of interest

The authors declare that they have no conflict of interest.

Founding

This work was supported by the National Science Centre, Poland [grant number 2017/27/N/ST8/02575] (grant author: M.Sc. Eng Paulina Kasprzyk); by the Czech Science Foundation (project 19-08549S); and by the Ministry of Education, Youth and Sports of Czech Republic, National Sustainability Program I-NPU I, Project POLYMAT LO1507.

References

Adkesson, D.N., Alsop, A.W., Ames, T.T., Chu, L.A., Disney, J.M., Dravis, B.C., Fitzgibbon, P., Gaddy, J.M., Gallagher, F.G., Lehnhardt, W.F., Lievense, J.C., Luyben, M.L., Seapan, M., Trotter, R.E., Wenndt, G.M., Yu, E.K., 2012. Purification of biologically-produced 1,3-propanediol. US8183417B2.

Beniah, G., Liu, K., Heath, W.H., Miller, M.D., Scheidt, K.A., Torkelson, J.M., 2016. Novel thermoplastic polyhydroxyurethane elastomers as effective damping materials over broad temperature ranges. Eur. Polym. J. 84, 770–783. https://doi.org/10.1016/J.EURPOLYMJ.2016.05.031

Buckley, C.P., Prisacariu, C., Martin, C., 2010. Elasticity and inelasticity of thermoplastic polyurethane elastomers: Sensitivity to chemical and physical structure. Polymer. 51, 3213–3224.

https://doi.org/10.1016/j.polymer.2010.04.069

Burk, M.J., Burgard, A.P., Osterhout, R.E., Sun, J., 2015. Microorganisms for the production of 1,4-butanediol. US20130109069A1.

Cervantes-Uc, J.M., Moo Espinosa, J.I., Cauich-Rodríguez, J.V., Avila-Ortega, A., Vazquez-Torres, H., Marcos-Fernández, A., San Roman, J., 2009. TGA / FTIR studies of segmented aliphatic polyurethanes and their nanocomposites prepared with commercial montmorillonites. Polym. Degrad. Stab. 94, 1666–1677. https://doi.org/10.1016/j.polymdegradstab.2009.06.022

de Oliveira, S.A., Nunes de Macedo, J.R., Rosa, D. dos S., 2019. Eco-efficiency of poly (lactic acid)-Starch-Cotton composite with high natural cotton fiber content: Environmental and functional value. J. Clean. Prod. 217, 32–41. https://doi.org/10.1016/j.jclepro.2019.01.198

Donato, R.K., Mija, A., 2019. Keratin Associations with Synthetic, Biosynthetic and Natural Polymers: An Extensive Review. Polymers. 12, 32. https://doi.org/10.3390/polym12010032

Duan, L., D'Hooge, D.R., Spoerk, M., Cornillie, P., Cardon, L., 2018. Facile and Low-Cost Route for Sensitive Stretchable Sensors by Controlling Kinetic and Thermodynamic Conductive Network Regulating Strategies. ACS Appl. Mater. Interfaces 10, 22678–22691. https://doi.org/10.1021/acsami.8b03967

Eceiza, A., Martin, M.D., de la Caba, K., Kortaberria, G., Gabilondo, N., Corcuera, M.A., Mondragon, I., 2008. Thermoplastic Polyurethane Elastomers Based on Polycarbonate Diols With Different Soft Segment Molecular Weight and Chemical Structure: Mechanical and Thermal Properties. Polym. Eng. Sci. 48, 297–306. https://doi.org/10.1002/pen

Emptage, M., Haynie, S.L., Laffend, L.A., Pucci, J.P., Whited, G.M., 2003. Process for the biological production of 1,3-propanediol with high titer. US6514733B1.

Fang, C., Zhou, X., Yu, Q., Liu, S., Guo, D., Yu, R., Hu, J., 2014. Synthesis and characterization of low crystalline waterborne polyurethane for potential application in water-based ink binder. Prog. Org. Coatings. 77, 61–71. https://doi.org/10.1016/j.porgcoat.2013.08.004

Ferg, E.E., Bolo, L.L., 2013. A correlation between the variable melt flow index and the molecular mass distribution of virgin and recycled polypropylene used in the manufacturing of battery

527 cases. Polym. Test. 32, 1452–1459. https://doi.org/10.1016/J.POLYMERTESTING.2013.09.009

528 Guerreiro, S.D.C., João, I.M., Pimentel Real, L.E., 2012. Evaluation of the influence of testing
529 parameters on the melt flow index of thermoplastics. Polym. Test. 31, 1026–1030.
530 https://doi.org/10.1016/J.POLYMERTESTING.2012.07.008

531 Herrera, M., Matuschek, G., Kettrup, A., 2002. Thermal degradation of thermoplastic polyurethane
532 elastomers (TPU) based on MDI. Polym. Degrad. Stab. 78, 323–331.
533 https://doi.org/10.1016/S0141-3910(02)00181-7

534 Hossieny, N., Shaayegan, V., Ameli, A., Saniei, M., Park, C.B., 2017. Characterization of hard-
535 segment crystalline phase of thermoplastic polyurethane in the presence of butane and glycerol
536 monosterate and its impact on mechanical property and microcellular morphology. Polymer. 112,
537 208–218. https://doi.org/10.1016/J.POLYMER.2017.02.015

538 Kasprzyk, P., Datta, J., 2019. Novel bio-based thermoplastic poly(ether-urethane)s. Correlations
539 between the structure, processing and properties. Polymer. 160, 1–10.
540 https://doi.org/10.1016/j.polymer.2018.11.032

541 Kasprzyk, P., Datta, J., 2018. Effect of molar ratio [NCO]/[OH] groups during prepolymer chains
542 extending step on the morphology and selected mechanical properties of final bio-based
543 thermoplastic poly(ether-urethane) materials. Polym. Eng. Sci. 58, E199 - E206.
544 https://doi.org/10.1002/pen.24874

545 Kasprzyk, P., Sadowska, E., Datta, J., 2019. Investigation of Thermoplastic Polyurethanes
546 Synthesized via Two Different Prepolymers. J. Polym. Environ. 27, 2588 - 2500.
547 https://doi.org/10.1007/s10924-019-01543-7

548 Kopczyńska, P., Datta, J., 2016. Single-phase product obtained via crude glycerine depolymerisation
549 of polyurethane elastomer: structure characterisation and rheological behaviour. Polym. Int. 65,
550 946–954. https://doi.org/10.1002/pi.5128

551 Król, P., 2007. Synthesis methods, chemical structures and phase structures of linear polyurethanes.
552 Properties and applications of linear polyurethanes in polyurethane elastomers, copolymers and
553 ionomers. Prog. Polym. Sci. 52, 915–1015. https://doi.org/10.1016/j.pmatsci.2006.11.001

554 Landim, L.B., Miranda, E.O., de Araújo, N.A., Pinto, J.C., Cabral-Albuquerque, E.C.M., Cunha, S.,
555 Fialho, R.L., 2019. Solvent-free mechanochemical polymerization of urea-succinic acid and urea-
556 succinic acid-glycerol mixtures. J. Clean. Prod. 238.
557 https://doi.org/10.1016/j.jclepro.2019.117742

558 Lee, Y.-H., Kang, B.-K., Kim, H.-D., Yoo, H.-J., Kim, J.-S., Huh, J.-H., Jung, Y.-J., Lee, D.-J., 2009.
559 Effect of hot pressing/melt mixing on the properties of thermoplastic polyurethane. Macromol.
560 Res. 17, 616–622. https://doi.org/10.1007/BF03218918

561 Lei, W., Fang, C., Zhou, X., Cheng, Y., Yang, R., Liu, D., 2017. Morphology and Thermal Properties of
562 Polyurethane Elastomer Based on Representative Structural Chain Extenders. Thermochim.
563 Acta. 653, 116 - 125. https://doi.org/10.1016/j.tca.2017.04.008

564 Lligadas, G., Ronda, J.C., Galia, M., Cadiz, V., 2013. Renewable polymeric materials from vegetable
565 oils : a perspective. Mater. Today. 16, 337–343. https://doi.org/10.1016/j.mattod.2013.08.016

566 Lvii, T., Ryszkowska, J., Urea-urethane, S., 2012. Supermolecular structure , morphology and physical
567 properties of urea-urethane elastomers. Polimery. 12, 775–902.

568 Ma, J., Harstvedt, J.D., Dunaway, D., Bian, L., Jaradat, R., 2018. An exploratory investigation of
569 Additively Manufactured Product life cycle sustainability assessment. J. Clean. Prod. 192, 55–70.
570 https://doi.org/10.1016/j.jclepro.2018.04.249

571 Mizera, K., Ryszkowska, J., 2016. Polyurethane elastomers from polyols based on soybean oil with a
572 different molar ratio. Polym. Degrad. Stab. 132, 21–31.
573 https://doi.org/10.1016/j.polymdegradstab.2016.05.004

574 Niemczyk, A., Piegat, A., Sonseca Olalla, Á., El Fray, M., 2017. New approach to evaluate microphase
575 separation in segmented polyurethanes containing carbonate macrodiol. Eur. Polym. J. 93, 182–
576 191. https://doi.org/10.1016/j.eurpolymj.2017.05.046

577 Parcheta, P., Datta, J., 2017. Environmental impact and industrial development of biorenewable
578 resources for polyurethanes. Crit. Rev. Environ. Sci. Technol. 47, 1986–2016.
579 https://doi.org/10.1080/10643389.2017.1400861

580 Pielichowski, K., Leszczy, A., 2004. TG-FTIR study of the thermal degradation of polyoxymethelene

(POM)/ thermoplastic polyurethane (TPU) blends. J. Therm. Anal. Calorim. 78, 631–637.

Prisacariu, C., 2011. Thermal behaviour of polyurethane elastomers, in: Polyurethane Elastomers. Springer Vienna, Vienna, pp. 61–101. https://doi.org/10.1007/978-3-7091-0514-6_3

Prisacariu, C., Scortanu, E., Agapie, B., 2013. Journal of Industrial and Engineering Chemistry Effect of the hydrogen bonding on the inelasticity of thermoplastic polyurethane elastomers. J. Ind. Eng. Chem. 19, 113–119. https://doi.org/10.1016/j.jiec.2012.07.012

Righetti, M.C., 2017. Crystallization of Polymers Investigated by Temperature-Modulated DSC. Materials. 10, 442–464. https://doi.org/10.3390/ma10040442

Saralegi, A., Rueda, L., Fernández-D'Arlas, B., Mondragon, I., Eceiza, A., Corcuera, M.A., 2013. Thermoplastic polyurethanes from renewable resources: Effect of soft segment chemical structure and molecular weight on morphology and final properties. Polym. Int. 62, 106–115. https://doi.org/10.1002/pi.4330

Verstraete, G., Van Renterghem, J., Van Bockstal, P.J., Kasmi, S., De Geest, B.G., De Beer, T., Remon, J.P., Vervaet, C., 2016. Hydrophilic thermoplastic polyurethanes for the manufacturing of highly dosed oral sustained release matrices via hot melt extrusion and injection molding. Int. J. Pharm. 506, 214–221. https://doi.org/10.1016/j.ijpharm.2016.04.057

Wang, S., Capoen, L., D'hooge, D.R., Cardon, L., 2017. Can the melt flow index be used to predict the success of fused deposition modelling of commercial poly(lactic acid) filaments into 3D printed materials? Plast. Rubber Compos. 47, 1–8. https://doi.org/10.1080/14658011.2017.1397308

Wirpsza, Z., 1993. Poliuretany: chemia, technologia, zastosowanie. WNT, Warszawa.

Xie, F., Zhang, T., Bryant, P., Colwell, J.M., Laycock, B., 2019. Degradation and stabilization of polyurethane elastomers. Prog. Polym. Sci. 90, 211–268. https://doi.org/10.1016/j.progpolymsci.2018.12.003

Xu, J., Wang, K., Sheng, H., Gao, M., Zhang, S., Tan, J., 2020. Energy efficiency optimization for ecological 3D printing based on adaptive multi-layer customization. J. Clean. Prod. 245, 118826. https://doi.org/10.1016/j.jclepro.2019.118826

607 Yang, H., Wang, X., Yu, B., Song, L., Hu, Y., Yuen, R.K.K., 2012. Effect of borates on thermal
608 degradation and flame retardancy of epoxy resins using polyhedral oligomeric silsesquioxane as
609 a curing agent. Thermochim. Acta. 535, 71–78. https://doi.org/10.1016/j.tca.2012.02.021

610 Yilgor, E., Atilla, G.E., Ekin, A., Kurt, P., Yilgor, I., 2003. Isopropyl alcohol: An unusual, powerful,
611 “green” solvent for the preparation of silicone-urea copolymers with high urea contents. Polymer
612 44, 7787–7793. https://doi.org/10.1016/j.polymer.2003.10.048

613 Yilgor, I., Yilgor, E., Guler, I.G., Ward, T.C., Wilkes, G.L., 2006. FTIR investigation of the influence of
614 diisocyanate symmetry on the morphology development in model segmented polyurethanes.
615 Polymer. 47, 4105–4114. https://doi.org/10.1016/j.polymer.2006.02.027

616

I STEP

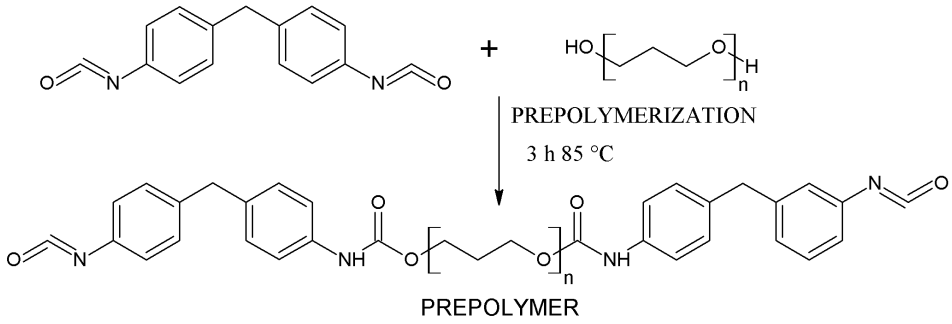

II STEP

a) extension of the prepolymer chains with using bio-BDO

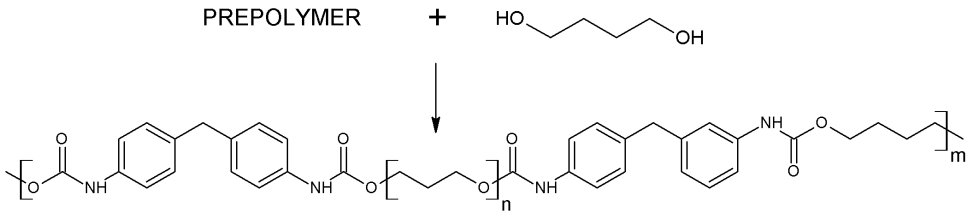

b) extension of the prepolymer chains with using bio-PDO

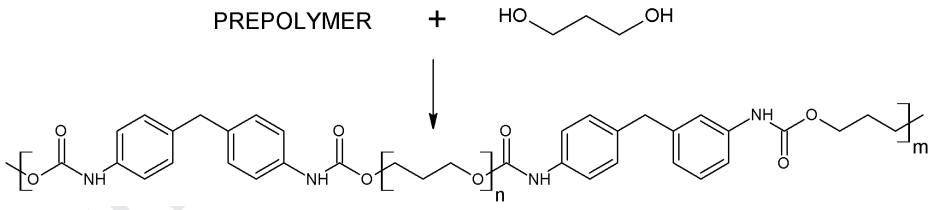

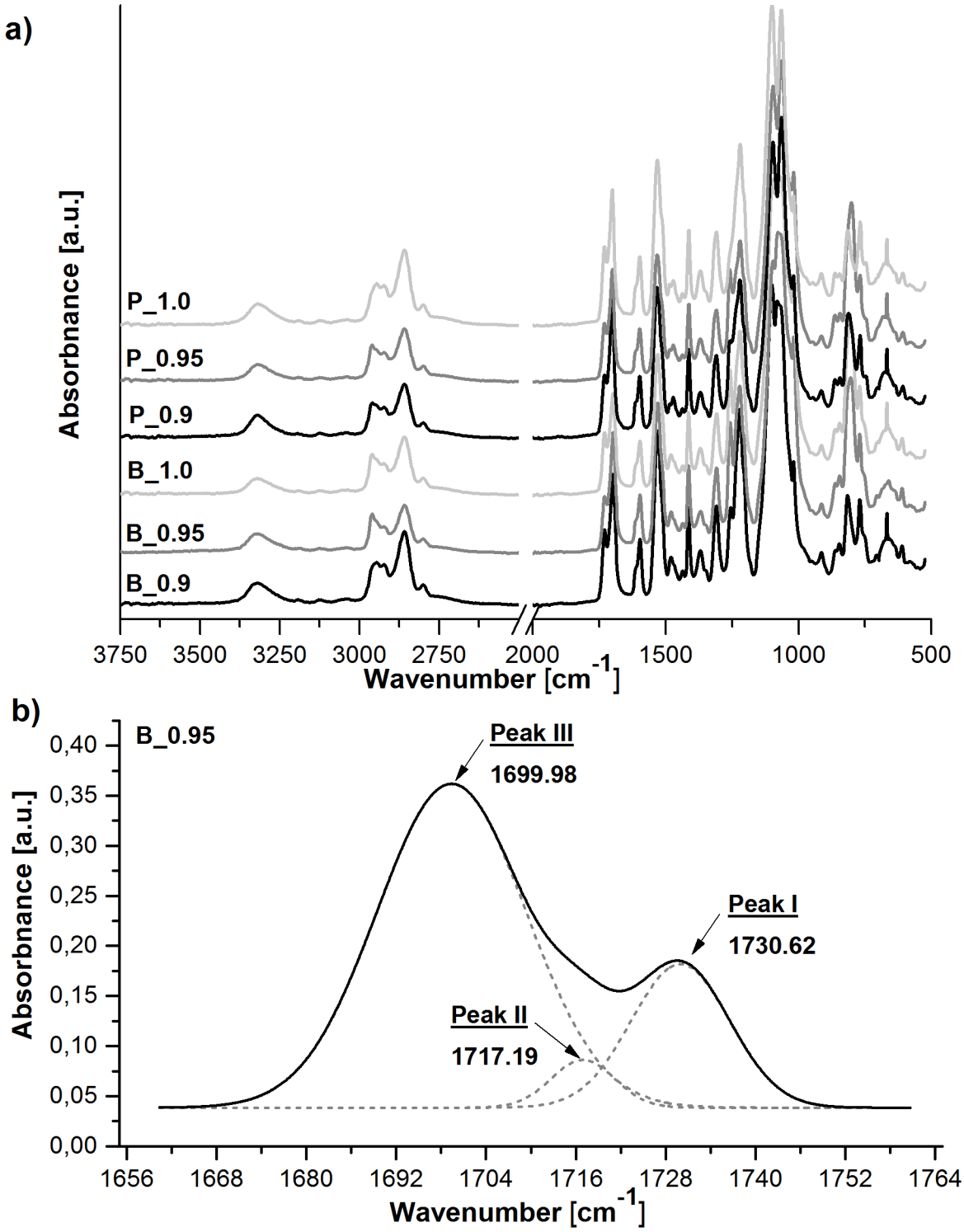
a)
Absorbnance [a.u.]
P_1.0
P_0.95
P_0.9
B_1.0
B_0.95
B_0.9
3750
3500
3250
3000
2750
2000
1500
1000
500
Wavenumber [cm-1]
b)
B_0.95
Peak III
1699.98
Peak I
1730.62
Peak II
1717.19
Absorbnance [a.u.]
0,40
0,35
0,30
0,25
0,20
0,15
0,10
0,05
0,00
1656
1668
1680
1692
1704
1716
1728
1740
1752
1764
Wavenumber [cm-1]

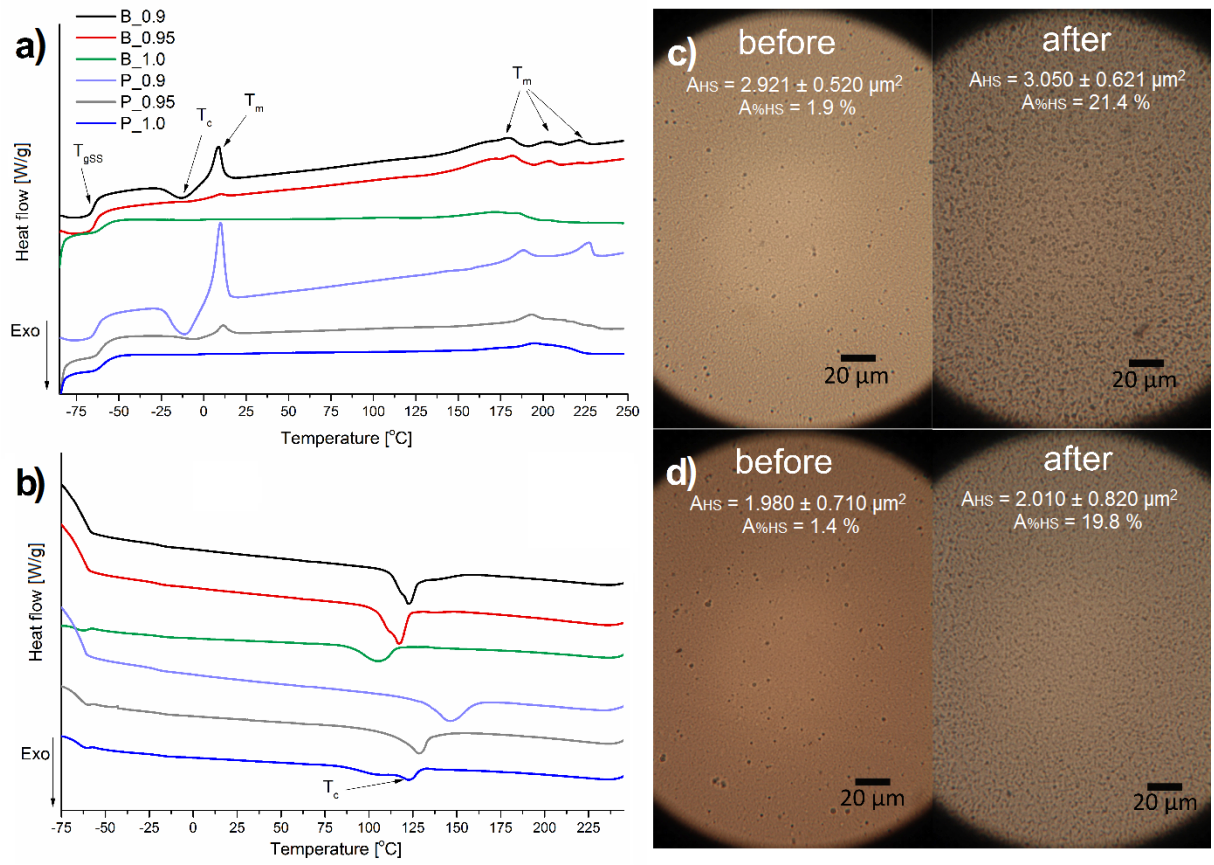
a)
B_0.9
B_0.95
B_1.0
P_0.9
P_0.95
P_1.0
T_{gSS}
T_c
T_m
T_m
Heat flow [W/g]
Exo
-75 -50 -25 0 25 50 75 100 125 150 175 200 225 250
Temperature [°C]
b)
Heat flow [W/g]
Exo
T_c
-75 -50 -25 0 25 50 75 100 125 150 175 200 225
Temperature [°C]
c)
before
A_{HS} = 2.921 ± 0.520 µm²
$A_{\%HS}$ = 1.9 %
20 µm
after
A_{HS} = 3.050 ± 0.621 µm²
$A_{\%HS}$ = 21.4 %
20 µm
d)
before
A_{HS} = 1.980 ± 0.710 µm²
$A_{\%HS}$ = 1.4 %
20 µm
after
A_{HS} = 2.010 ± 0.820 µm²
$A_{\%HS}$ = 19.8 %
20 µm

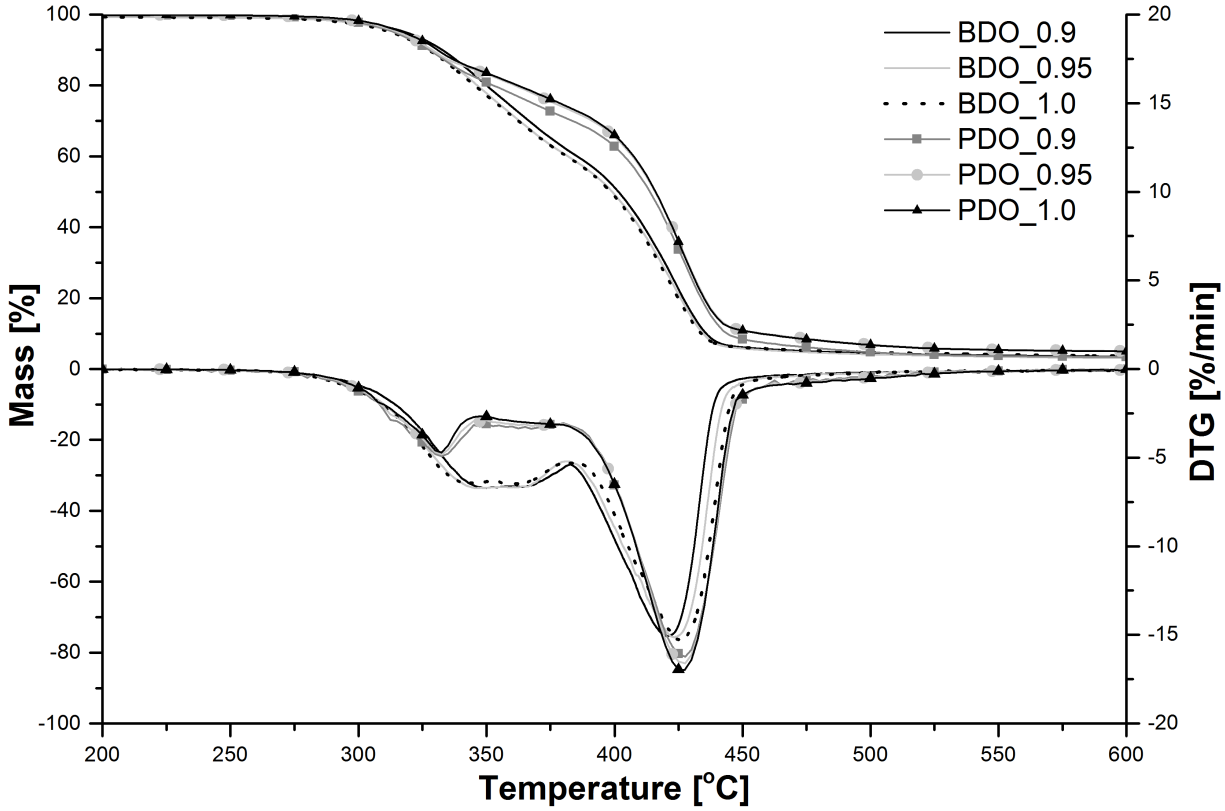
BDO_0.9
BDO_0.95
BDO_1.0
PDO_0.9
PDO_0.95
PDO_1.0
Mass [%]
DTG [%/min]
Temperature [°C]
100
80
60
40
20
0
-20
-40
-60
-80
-100
20
15
10
5
0
-5
-10
-15
-20
200
250
300
350
400
450
500
550
600

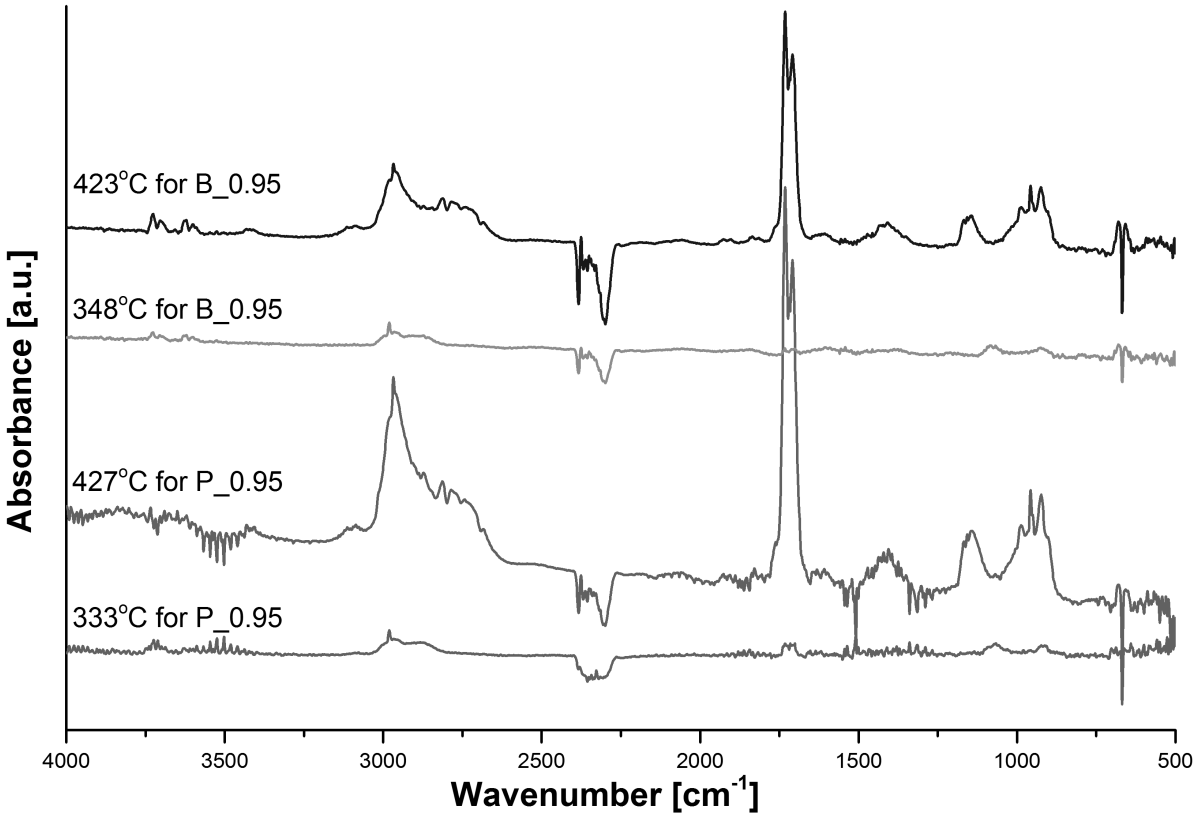
423°C for B_0.95
348°C for B_0.95
427°C for P_0.95
333°C for P_0.95
Absorbance [a.u.]
4000
3500
3000
2500
2000
1500
1000
500
Wavenumber [cm-1]

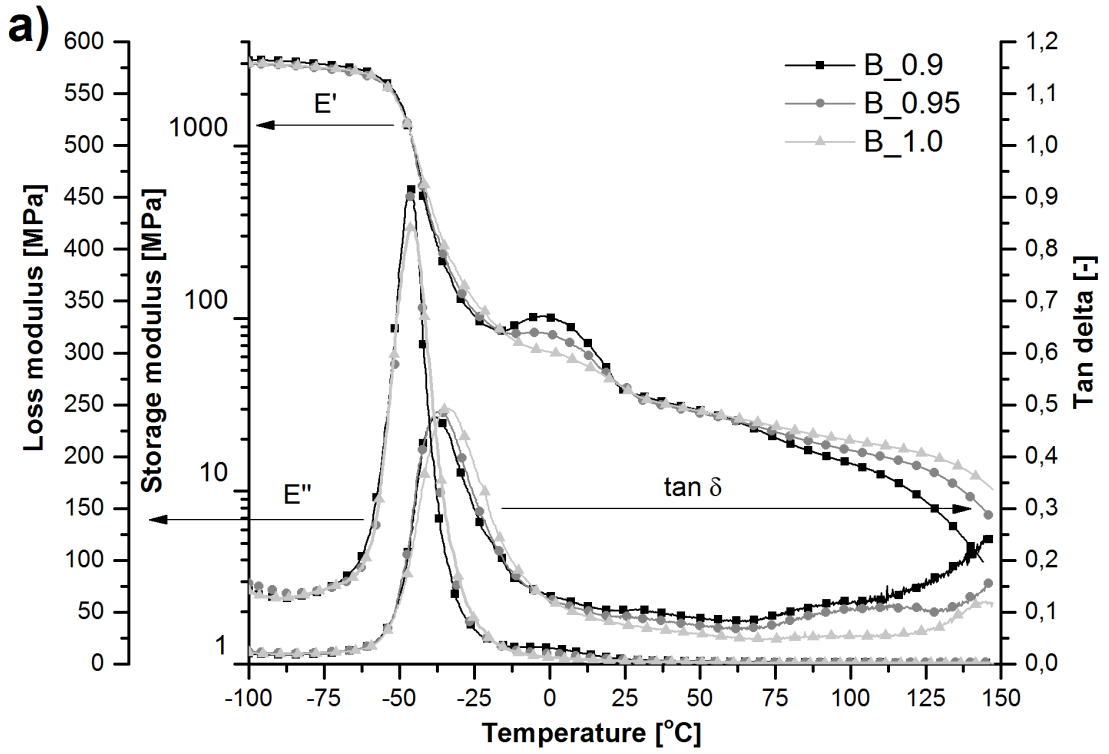
a)
B_0.9
B_0.95
B_1.0
E'
E''
tan δ
Loss modulus [MPa]
Storage modulus [MPa]
Tan delta [-]
Temperature [°C]

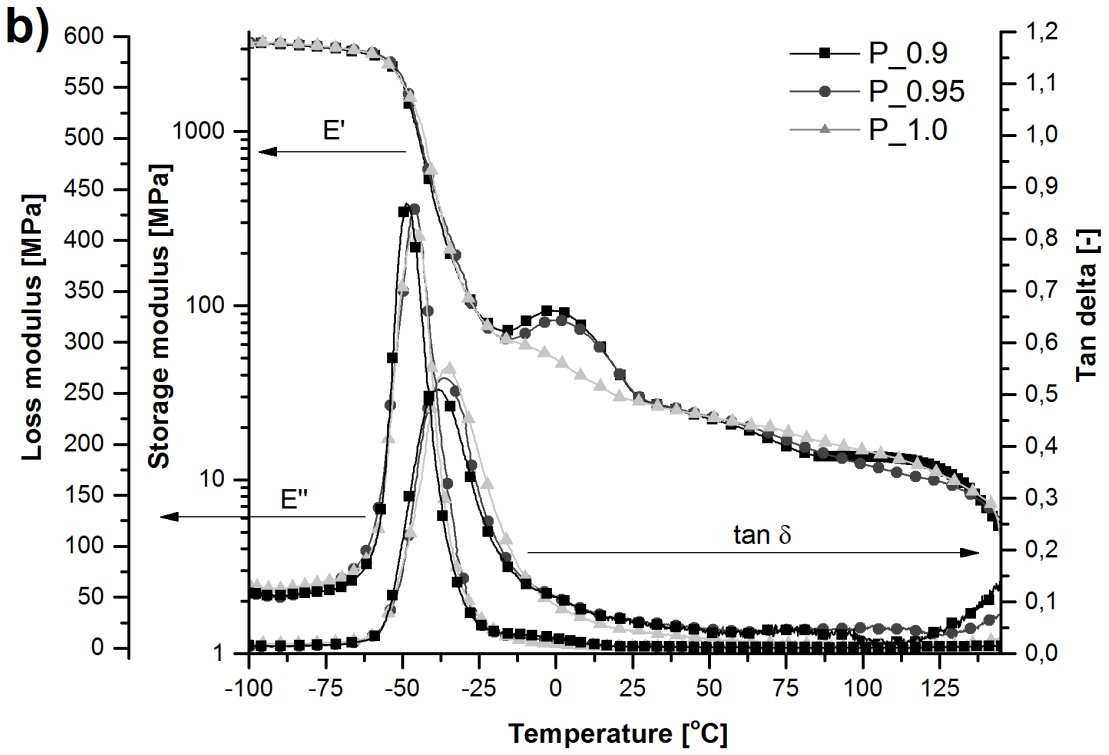
b)
P_0.9
P_0.95
P_1.0
E'
E''
tan δ
Loss modulus [MPa]
Storage modulus [MPa]
Tan delta [-]
Temperature [°C]

a)

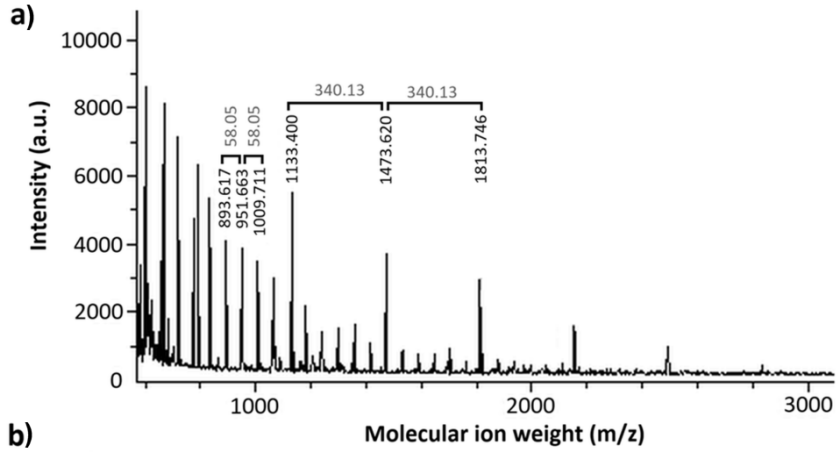

b)

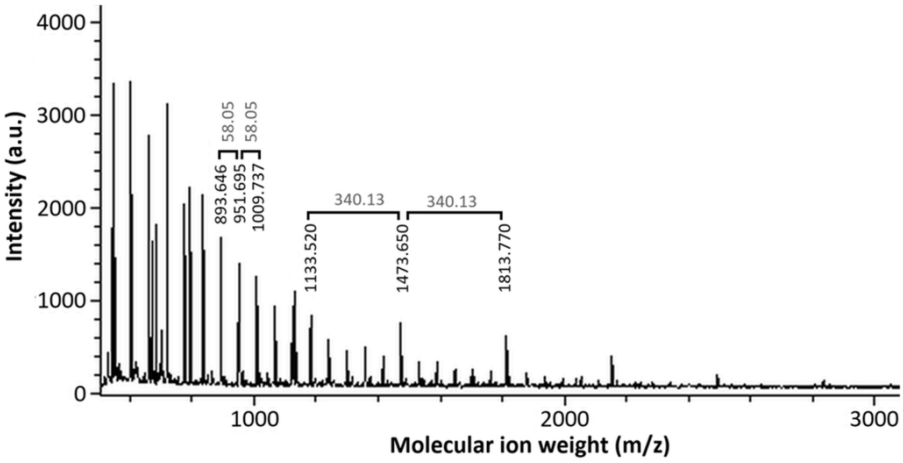

c)

Sample	M_{pI}	M_{pII}	M_{pIII}	M_{pIV}	M_{pV}	M_{pVI}
B_0.9	42153 (95.9%)	2353 (1.4%)	1528 (1.9%)	786 (0.7%)	450 (0.1%)	225 (0.003%)
B_0.95	53239 (96.9%)	2384 (0.9%)	1541 (1.3%)	750 (0.6%)	442 (0.3%)	- -

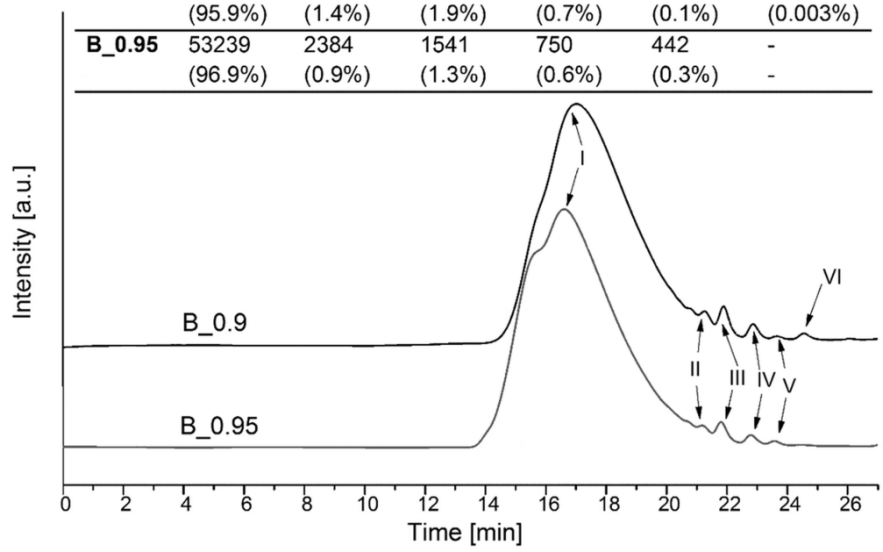

Figure captions

Figure 1. The synthesis of bio-based thermoplastic TPUs.

Figure 2. a) FTIR-ATR spectra of bio-based TPU systems, b) Gauss model fitting of sample B_0.95. The solid line represents the sum of the overlapped peak-components (I – III), and the dashed lines represent the deconvoluted distributions.

Figure 3. DSC thermal transition curves of the second heating (a) and first cooling (b) ramps of the bio-based TPUs. POM microphotographs of samples B_0.9 (c), and B_0.95 (d), before (left) and after (right) a thermal treatment at 250 °C (under vacuum) followed by a controlled cooling at 2 °C/min. AHS is the area and A%HS is the area fraction (and an estimation of the volume fraction) of HS aggregates.

Figure 4. TGA and DTG curves of the bio-based TPUs.

Figure 5. FTIR spectra recorded during the 1st and 2nd mass loss step for the bio-TPU systems B_0.95 and P_0.95**.**

Figure 6. DMTA curves of the TPUs based on (a) bio-BDO and (b) bio-PDO as a function of the temperature.

Figure 7. MALDI-TOF spectra of systems a) B_0.9 and b) B_0.95 highlighting the repetitive low molecular mass units representing monomeric/oligomeric species in the final TPUs, and c) SEC results of systems B_0.9 and B_0.95, where M_{pn} represents M_n (g/mol) of the nth peak.

Highlights

- Available H-bond donor groups improve interphase bonding.

- Tunability between hard and soft TPU segments based on the [NCO]/[OH] molar ratio.

- Broad processability range, including in ideal range for FDM additive manufacturing.